Generalized Resilience and Failure Indices for Use with Pressure-Driven Modeling and Leakage

Enrico Creaco[1]; Marco Franchini[2]; and Ezio Todini[3]

Abstract: In 2000, the resilience and failure indices were introduced as a convenient and compact tool to express respectively water-distribution network (WDN) surplus and deficit in satisfying users' demand, in terms of delivered power. In their original formulation, the mentioned indices, originally thought as WDN design tools, were developed only considering the demand-driven modeling approach, which would include pumps but not leakage. This paper extends the formulation of both indices and presents a generalized expression, more convenient for use when dealing with pressure-driven modeling and capable of including the effect of leakage. Following the original concept, the generalized indices were developed by calculating the power dissipated in the network as a function of the difference between the total power inserted through source nodes and pumps and the net delivered power, whereas the leakage-related power is considered as a loss similarly to the internally dissipated one. Applications to WDN analysis and design proved that using the new formulation in the presence of leakage and pressure-dependent consumptions yields better description of the delivered power excess, compared to the original demand-driven formulation and to another pressure-driven formulation present in the scientific literature. **DOI: 10.1061/(ASCE)WR.1943-5452.0000656.**

Author keywords: Resilience; Failure; Reliability; Water distribution modeling; Design; Simulation.

Introduction

Water-distribution network (WDN) reliability is often described and assessed through suitable performance indicators (Gargano and Pianese 2000; Tanyimboh et al. 2001; Ciaponi 2009; Creaco and Franchini 2012). These indicators relate the water discharges delivered to network users, to their demands under critical operational scenarios, which occur due to either mechanical (pipe breakage, pump failure, power outages, control valve failure, etc.) or hydraulic (such as changes in demand or in pressure head, aging of pipes, inadequate pipe sizing, insufficient pumping capacity, insufficient storage capability) failure (Mays 1996). An overall measure of reliability is then obtained by averaging the performance indicators calculated in each category of critical scenarios (Ciaponi 2009). As an example, if the network reliability related to pipe breakage is considered, the ratio of delivered water discharge to users' demand has to be assessed for each possible pipe break in the network, as done by Giustolisi et al. (2008a) and Creaco et al. (2012). Apart from identifying the segment that includes the generic broken pipe and the network part that remains connected to the source following the segment isolation, this requires performance of one pressure-driven simulation for each network segment. Though applying this procedure is not a heavy task in the analysis of WDNs, it may turn out to be too cumbersome in the optimization context, when it has to be reiterated for each solution proposed by the optimizer.

To avoid using performance indicators in the optimization context, various researchers have tried to formulate compact indices of reliability, which require a single network simulation for being evaluated while being good surrogates for the more cumbersome performance indicators. In this context, the pressure head/energy related indices, such as the pressure surplus by Gessler and Walski (1985) and the resilience index by Todini (2000), aim to express the network reliability in terms of service pressure excess compared to the minimum desired value guaranteeing the full demand satisfaction. In particular, the resilience index by Todini (2000) is calculated taking as benchmark a network configuration that delivers network demands with the minimum desired pressure head value at all nodes. In particular, it is the ratio of the excess of power delivered to users, to the maximum power that can be dissipated in the network when satisfying the demand. Incidentally, the latter corresponds to the total power introduced into the network through the source nodes and eventually present pumps minus the minimum power necessary to satisfy the demand. Later, some authors (e.g., Prasad et al. 2003; Raad et al. 2010; Pandit and Crittenden 2012; Cimellaro et al. 2015) proposed other definitions of the resilience index. In particular, Prasad et al. (2003) and Raad et al. (2010) incorporated into the original index by Todini (2000) the uniformity of pipe diameters and water discharges respectively, in order to obtain a better representation of network reliability. However, these modified versions have the drawback of corrupting the original physical meaning of the resilience index. To preserve this physical meaning while taking account of the uniformity of pipe sizes in the WDN, Creaco et al. (2015) proposed using an additional loop diameter uniformity index, along with the original resilience index, in the optimization context. Their calculations proved that dealing with resilience index and loop diameter uniformity as separate objective functions helps in obtaining a more comprehensive representation of the network reliability. Nevertheless, despite positive correlation with reliability (Atkinson et al. 2014), the resilience index is a global index and, as such, can only give an overall and

[1]Assistant Professor, Dipartimento di Ingegneria Civile e Architettura, Univ. of Pavia, Via Ferrata 3, 27100 Pavia, Italy (corresponding author). E-mail: creaco@unipv.it

[2]Professor, Dipartimento di Ingegneria, Univ. of Ferrara, Via Saragat 1, 44100 Ferrara, Italy. E-mail: marco.franchini@unife.it

[3]Retired, Professor, President of Italian Hydrological Society, Piazza di Porta San Donato, 40126 Bologna, Italy. E-mail: ezio.todini@gmail.com

Note. This manuscript was submitted on October 21, 2015; approved on January 7, 2016No Epub Date. Discussion period open until 0, 0; separate discussions must be submitted for individual papers. This paper is part of the ***Journal of Water Resources Planning and Management***, © ASCE, ISSN 0733-9496.

approximate description of the network operating conditions. In fact, the local demand shortfalls that occur under the usual operating conditions or critical scenarios, such as those associated with segment isolation or open hydrant(s), cannot be detected through the resilience index and require the burdensome calculation of performance indicators.

With the objective to design a WDN, the resilience index, as proposed by Todini (2000), was formulated in the context of demand-driven modeling (Todini and Pilati 1988), where nodal water discharges are assumed always equal to nodal demands and leakage cannot be accounted for but in an approximate way. Indeed, a generalization to the pressure-driven modeling (Germanopoulos 1985; Wagner et al. 1988; Reddy and Elango 1989; Gupta and Bhave 1996; Tucciarelli et al. 1999; Tanymboh et al. 2001; Alvisi and Franchini 2006; Giustolisi et al. 2008b) has already been recently proposed by Saldarriaga et al. (2010). However, this approach, which does not fully follow the original concept, has the drawback of including leakage outflows in the numerator of the proposed resilience index. This may result in an undesired increase in the index as leakage grows, as if leakage were something good that needs to be recovered.

Following the original definition, this paper presents a generalized expression of the resilience index to pressure-driven modeling, which is able to incorporate both leakage and pressure dependent outflows to users in a robust and sound way. Along with the resilience index, the failure index, originally proposed by Todini (2000), which concerns the system supplied power under pressure deficit operating conditions, is also generalized as an extension to the negative values of the resilience index. In the following sections, first the methodology is described, reporting the pressure-driven modeling used for the calculations and the form of the generalized resilience and failure indices. The results that prove the applicability of the indices in both the analysis and the optimization contexts follows.

Methodology

Pressure-Driven Modeling Approach

Let us assume a generic network with n_0 source nodes with preassigned head and n_1 nodes with unknown head. Furthermore, let the network include n_p pipes and n_{pumps} pumps. In network resolution, vector $\mathbf{H_0}$ $(n_0 \times 1)$ of preassigned heads (i.e., heads at the source nodes, reservoirs or tanks) and vector $\mathbf{d}$ $(n_1 \times 1)$ of demands at the n_1 unknown head nodes are generally known at each instant of network operation. In particular, in the case of a reservoir, the generic head H_0 is generally preassigned. In the case of a tank, instead, it is determined based on the series of tank inflows and outflows by applying the continuity equation to the tank. The generic nodal demand d is estimated by applying either the top-down or the bottom-up demand allocation approaches to the network users (Walski et al. 2003). Network resolution enables vectors $\mathbf{Q}$ $(n_p \times 1)$, $\mathbf{Q_p}$ $(n_{\text{pumps}} \times 1)$ and $\mathbf{H}$ $(n_1 \times 1)$, associated with pipe water discharges, pump water discharges and unknown nodal heads respectively, to be calculated. This is accomplished by applying the following momentum and continuity equations to the n_p network pipes and n_{pumps} network pumps, and to the n_1 network nodes, respectively:

5

$$\begin{cases} \mathbf{A_{11}Q} + \mathbf{A_{12}H} = -\mathbf{A_{10}H_0} & \text{momentum equation along pipes} \\ -\mathbf{A_{pp}Q_p} + \mathbf{A_{p2}H} = -\mathbf{A_{p0}H_0} & \text{momentum equation along pumps} \\ \mathbf{A_{21}Q} + \mathbf{A_{2p}Q_p} = \mathbf{q} & \text{continuity equation} \end{cases} \tag{1}$$

where matrices $\mathbf{A_{12}}$ $(n_p \times n_1)$, $\mathbf{A_{10}}$ $(n_p \times n_0)$, $\mathbf{A_{p2}}$ $(n_{\text{pumps}} \times n_1)$ and $\mathbf{A_{p0}}$ $(n_{\text{pumps}} \times n_0)$ are obtained from topological incidence matrix $\mathbf{A}$ $[(n_p + n_{\text{pumps}}) \times n]$. The generic row of the latter matrix helps distinguishing the upstream and downstream nodes of the generic network link (corresponding matrix values equal to -1 and 1, respectively) from the network nodes not belonging to the link (corresponding matrix value equal to 0). In particular, $\mathbf{A_{12}}$ $(n_p \times n_1)$ is derived by extracting the rows associated with the n_p pipes and the columns associated with the n_1 unknown head nodes. $\mathbf{A_{10}}$ $(n_p \times n_0)$ is derived by extracting the rows associated with the n_p pipes and the columns associated with the n_0 preassigned head nodes. $\mathbf{A_{p2}}$ $(n_{\text{pumps}} \times n_1)$ is derived by extracting the rows associated with the n_{pumps} pumps and the columns associated with the n_1 unknown head nodes. Finally, $\mathbf{A_{p0}}$ $(n_{\text{pumps}} \times n_0)$ is derived by extracting the rows associated with the n_{pumps} pumps and the columns associated with the n_0 preassigned head nodes.

Matrices $\mathbf{A_{21}}$ and $\mathbf{A_{2p}}$ are the transpose matrices of $\mathbf{A_{12}}$ and $\mathbf{A_{p2}}$ respectively.

$\mathbf{A_{11}}$ $(n_p \times n_p)$ is a diagonal matrix, whose elements identify the resistances of the n_p network pipes through the following relationship:

$$A_{11}(i,i) = \frac{b_i |Q_i|^{\alpha-1} L_i}{k_i^{\gamma} D_i^{\beta}} + \frac{8\xi}{g\pi^2} \frac{|Q_i|}{D_i^4} \tag{2}$$

where D_i = diameter of the ith pipe and where roughness coefficient k_i, coefficient b_i and exponents α, β, and γ depend on the formula used to express pipe head losses. Furthermore, ξ = local headloss coefficient, which also enables accounting for the presence of valves in the pipe, g = gravity acceleration (approximately set equal to 9.81 ms^{-2}) and π ~~the~~ ratio of a circle's circumference to its diameter (approximately set equal to 3.14).

In Eq. (1) $\mathbf{A_{pp}}$ $(n_{\text{pumps}} \times n_{\text{pumps}})$ is a diagonal matrix, whose generic element $A_{pp}(i,i)$ expresses the ratio of head H_p to water discharge Q_p for the ith pump

$$A_{pp}(i,i) = \frac{c_{i,1} Q_{p,i}^2 + c_{i,2} Q_{p,i} + c_{i,3}}{|Q_{p,i}|} \tag{3}$$

where $c_{i,1}$, $c_{i,2}$, and $c_{i,3}$ = pump curve coefficients. Eq. (3) holds valid also when the pump works as a turbine or when the device installed in the pipe is a turbine. In the cases when the manufacturer provides the pump curve in graphical form, regression techniques can be applied to derive the best fit coefficient c_i values for the quadratic form in Eq. (3).

Vector $\mathbf{q}$ $(n_1 \times 1)$ in Eq. (1) is the vector of the outflows at the n_1 unknown head nodes. In the demand-driven approach (Todini and Pilati 1988), this vector is set equal to vector $\mathbf{d}$ of nodal demands. In this case, leakage can be included in d only in an approximate way, without any relationship with the nodal heads. In the pressure-driven modeling approach, instead, the nodal outflow is assessed as a function of the nodal demand and pressure head, and leakage can be accurately modeled. Vector $\mathbf{q}$ is calculated as

$$\mathbf{q} = \mathbf{q_{user}} + \mathbf{q_{leak}} \tag{4}$$

where $\mathbf{q_{user}}$ $(n_1 \times 1)$ and $\mathbf{q_{leak}}$ $(n_1 \times 1)$ represent the outflow delivered to the users and the leakage allocated to the nodes. The relationship between $\mathbf{q_{user}}$, $\mathbf{d}$, and $\mathbf{h}$ takes on the following form:

$$\mathbf{q_{user}} = \mathbf{C_{user}d} \tag{5}$$

where matrix $\mathbf{C_{user}}$ = diagonal matrix, whose generic element $C_{\text{user}}(i,i)$ expresses the outflow/demand ratio q_{user}/d for the users at the ith node.

According to the formulation by Wagner et al. (1988), which finds its mathematical expression in Eq. (6), this ratio is equal to 0 (i.e., nodal outflow $q_{\text{user}} = 0$) as long as the nodal pressure head is lower than or equal to a threshold value $h_{\min}$. Starting from $h_{\min}$, the ratio increases up to a value equal to 1, which means outflow q_{user} equal to users' demand, achieved when the nodal pressure head equals the threshold desired value h_{des}. For nodal pressure heads higher than h_{des}, the ratio stays equal to 1, with the users' demand being fully satisfied

$$C_{\text{user}}(i,i) = \begin{cases} 0 & \text{if } 0 \leq h_i \leq h_{\min} \\ \left(\dfrac{h_i - h_{\min}}{h_{\text{des}} - h_{\min}}\right)^{\delta} & \text{if } h_{\min} \leq h_i \leq h_{\text{des}} \\ 1 & \text{if } h_{\text{des}} \leq h_i \end{cases} \quad (6)$$

The exponent δ in Eq. (6) is generally set to 0.5.

Following the Germanopoulos (1985) formulation, leakage Q_{Li} in the ith pipe, to be allocated to either end node, can be calculated as

$$Q_{Li} = C_{L,i} L_i h_{a,i}^{n_{\text{leak}}} \quad (7)$$

where $C_{L,i}$, L_i, and $h_{a,i}$ = leakage coefficient, the length and the average pressure head in the generic pipe, respectively; n_{leak} = leakage exponent, which generally takes on values within the range [0.5, 1.5] (Van Zyl and Cassa 2014). Vector $\mathbf{q_{leak}}$ of leakage allocated to the unknown head nodes can be expressed in the following compact vector form, derived from Creaco and Pezzinga (2015b, a):

$$\mathbf{q_{leak}} = \frac{|\mathbf{A_{21}}|\text{diag}(\mathbf{CLL})}{2}\left(\frac{|\mathbf{A_{10}}|\,\mathbf{h_0} + |\mathbf{A_{12}}|\,\mathbf{h}}{2}\right)^{n_{\text{leak}}} \quad (8)$$

where $\mathbf{CLL}(n_p \times 1)$ = vector whose ith element is equal to $C_{L,i}L_i$, and $\mathbf{h}$ $(n_1 \times 1)$ and $\mathbf{h_0}$ $(n_0 \times 1)$ = vector of pressure heads in the unknown and fixed head nodes, respectively. Incidentally, these vectors can be obtained from $\mathbf{H}$ and $\mathbf{H_0}$, by subtracting $\mathbf{z}$ $(n_1 \times 1)$ and $\mathbf{z_0}$ $(n_1 \times 1)$, vectors of ground elevations for the unknown and fixed head nodes, respectively. In Eq. (8), the division by 2 and the exponent n_{leak} apply to each element of the matrices.

Resilience and Failure Indices in the Pressure-Driven Modeling Approach

The resilience (I_{rd}) and failure (I_{fd}) indices originally defined by Todini (2000) through the *demand-driven modeling approach* take on the following form, using the notation of this paper:

$$I_{rd} = \frac{\max[\mathbf{d^T}(\mathbf{H} - \mathbf{H_{des}}), 0]}{\mathbf{Q_0^T H_0} + \mathbf{Q_p^T H_p} - \mathbf{d^T H_{des}}} \quad (9)$$

$$I_{fd} = \frac{\min[\mathbf{d^T}(\mathbf{H} - \mathbf{H_{des}}), 0]}{\mathbf{d^T H_{des}}} \quad (10)$$

Whereas the failure index has never been generalized to the pressure-driven modeling, a generalization of the resilience index was proposed by Saldarriaga et al. (2010) in the presence of leakage and in the absence of pumps. In particular, using the notation of this paper, the Saldarriaga et al. (2010) resilience index I_{rs} (where s stands for Saldarriaga) takes on the following form:

$$I_{rs} = \frac{(\mathbf{q_{user}} + \mathbf{q_{leak}})^{\mathbf{T}}(\mathbf{H} - \mathbf{H_{des}})}{\mathbf{Q_0^T H_0} - (\mathbf{q_{user}} + \mathbf{q_{leak}})^{\mathbf{T}}\mathbf{H_{des}}} \quad (11)$$

Eq. (11) has the drawback of putting the vector of leakage outflows in the numerator, as if it were something good that would need to be recovered.

Hereinafter, the resilience and failure indices are generalized to the pressure-driven approach avoiding the flaw mentioned previously.

As a generalization of Todini (2000), the resilience index can be calculated as

$$I_r = 1 - \frac{P_{\text{int}}^*}{P_{\max}^*} \quad (12)$$

where $P_{\text{int}}^* = \gamma(\mathbf{Q_0^T H_0} + \mathbf{Q_p^T H_p} - \mathbf{q_{user}^T H})$ = actual amount of power dissipated in the network, through pipe resistances and leakage outflow, to supply the users; vector $\mathbf{q_{user}}$ is evaluated through Eqs. (5) and (6), and $\mathbf{Q_0}$ $(n_0 \times 1)$ = vector of water discharges leaving the source nodes (thus including leakages as well). $P_{\max}^* = \gamma(\mathbf{Q_o H_0} + \mathbf{Q_p^T H_p} - \mathbf{d^T H_{des}})$ is, instead, the maximum power that would be dissipated in the network, under the theoretical condition of $\mathbf{q_{user}} = \mathbf{d}$ and $\mathbf{H} = \mathbf{H_{des}} = \mathbf{z} + \mathbf{h_{des}}$ at all network nodes.

Following algebraic operations, the following relationship is obtained:

$$I_r = \frac{\mathbf{q_{user}^T H} - \mathbf{d^T H_{des}}}{\mathbf{Q_0^T H_0} + \mathbf{Q_p^T H_p} - \mathbf{d^T H_{des}}} \quad (13)$$

Implicitly, it has to be underlined that $\mathbf{Q_p^T H_p}$ in Eq. (13) also accounts for pumps working as turbines or turbines themselves installed in the WDN. In the case of pumps working as turbines and/or turbines, the generic value $Q_p H_p$ is *negative*, i.e., the device takes energy out of the WDN. In a similar way, for network tanks that receive water from the network, instead of releasing it, negative values of $Q_0 H_0$ would be obtained.

Network configurations for which $\mathbf{q_{user}^T H} < \mathbf{d^T H_{des}}$ [i.e., they have negative numerator in Eq. (13)] are unsatisfactory in terms of power delivered to users. In fact, they have a deficit of power, rather than a surplus with respect to what is *desired*. Since the resilience index is meant to describe network redundancy, this index can be set to 0 for these networks. This results in the following relationship, which can be universally used for assessing the resilience index:

$$I_r = \frac{\max(\mathbf{q_{user}^T H} - \mathbf{d^T H_{des}}, 0)}{\mathbf{Q_0^T H_0} + \mathbf{Q_p^T H_p} - \mathbf{d^T H_{des}}} \quad (14)$$

Please note that $\mathbf{q_{user}}$, $\mathbf{H}$, $\mathbf{Q_0}$ and $\mathbf{Q_p}$ have to be computed through a *pressure-driven modeling approach*. The function max in Eq. (14) is useful for getting a value of the resilience index I_r equal to 0 in those network configurations that features a power deficit rather than a power surplus. Without this function, i.e., if I_r were expressed like in Eq. (13), these configurations would feature illogical values of I_r (sometimes even smaller than -1 or larger than 1), as will be shown in the applications. By inserting the max function, instead, the configurations with power deficit are assigned a null value of I_r, while the entity of the power deficit is properly described through the failure index, whose definition follows.

Written as in Eq. (14), the resilience index always ranges from 0 to 1, for all the kinds of networks. The highest value of $I_r = 1$ is obtained for a theoretical network configuration with no leakage and energy dissipations along the pipes.

In a similar way, the failure index originally proposed by Todini (2000) can be generalized through the following relationship:

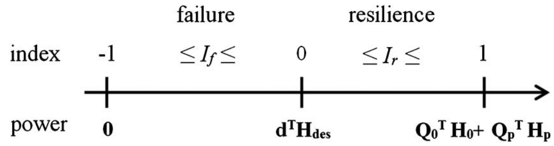

Fig. 1. Ranges of validity for the resilience and failure indices in terms of values of power/γ delivered to the users

$$I_f = \frac{\min(\mathbf{q}_{\mathbf{user}}^{\mathbf{T}}\mathbf{H} - \mathbf{d}^{\mathbf{T}}\mathbf{H}_{\mathbf{des}}, 0)}{\mathbf{d}^{\mathbf{T}}\mathbf{H}_{\mathbf{des}}} \tag{15}$$

Here, again, the quantities $\mathbf{q}_{\mathbf{user}}$ and $\mathbf{H}$ have to be computed through a *pressure-driven modeling approach.* The function min in Eq. (15) is useful for getting a value of the failure index I_f equal to 0 in the network configurations that feature a power surplus rather than a power deficit and are better described through I_r.

Written as in Eq. (15), the failure index always takes on values ranging from −1 to 0, for all the kinds of networks. In particular, values equal to 0 are obtained for network with no deficit of power, i.e., those that feature positive values of I_r. Values lower than 0, instead, are obtained for networks with deficit of power, i.e., those that feature a value of $I_r = 0$. The lowest possible value $I_f = -1$ is obtained when $\mathbf{q}_{\mathbf{user}} = \mathbf{0}$, with $\mathbf{0}$ being the zero vector, i.e., in a network supplying no water to all its users due to low service pressure conditions.

The main difference between the generalized resilience and failure indices [Eqs. (14) and (15)], on the one hand, and the original ones [Eqs. (9) and (10)], on the other hand, lies in the numerator of the former, where the vector $\mathbf{q}_{\mathbf{user}}$ of nodal outflows to users appears instead of the vector $\mathbf{d}$ nodal demands. Again, variables $\mathbf{H}$ and $\mathbf{Q_0}$ in [Eqs. (14) and (15)] are derived through pressure-driven modeling, whereas the corresponding ones in [Eqs. (9) and (10)] are obtained through demand-driven modeling.

The continuity of I_r and I_f is shown in Fig. 1, as a function of power $\mathbf{q}_{\mathbf{user}}^{\mathbf{T}}\mathbf{H}$ delivered to the WDN users. As formulated in this work, the indices are nonnegative and nonpositive respectively. Furthermore, either index takes on values different from 0 if and only if the other is equal to 0. In light of this continuity, a generalized resilience/failure index (GRF) GRF $= I_r + I_f$ can be used to give indications of the WDN power surplus/deficit. As a result of the definition of I_r and I_f, GRF equals I_r, when the latter is larger than 0. Otherwise, for network configurations under deficient power conditions for which $I_r = 0$, GRF is equal to the failure index I_f, which always takes on nonpositive values. Index GFR can be profitably used in the optimization context, as will be shown hereinafter.

Snapshot Simulation and Extended Period Simulation

When a single scenario is chosen as benchmark, assessment of the resilience and failure indices is easily done through Eqs. (14) and (15), respectively. In the case of extended period simulation, a single value can be calculated for either index at each network operation instant. Wherefore, the characterization of the whole operation period can be carried out by calculating, for either index, the temporal average or the minimum, median, and maximum values. The cumulative Weibull frequency of either index can also be estimated.

Applications

Case Studies

Applications concerned three different case studies—a synthetic case study (Fig. 2) and two real case studies of different complexity (Figs. 3 and 4). Given that the focus of this paper is mainly the assessment of the benefits of the new extended resilience index formulation, water demand is assumed perfectly known and the usual network operation with no failure is considered in all the case studies. Furthermore, when network design is performed, it is done in one step, without considering the phasing of construction in time (see Creaco et al. 2014).

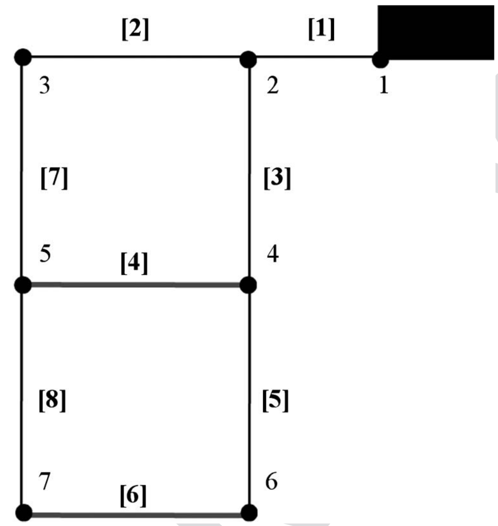

Fig. 2. First case study: network of Alperovits and Shamir (1977); node IDs close to the nodes; pipe IDs inside the brackets [] (adapted from Alperovits and Shamir 1977)

The first case study is the simple network of Alperovits and Shamir (1977), made up of $n_1 = 6$ nodes with unknown head, $n_0 = 1$ node with preassigned head, $n_p = 8$ pipes and no pumps (Fig. 2). The network was analyzed in a snapshot scenario representative of the peak demand. As in the original paper, a Hazen Williams roughness coefficient equal to 130 $\mathrm{m}^{0.37}\ \mathrm{s}^{-1}$ was used for all network pipes. The data relative to the preassigned head at the source node, nodal demands and pipe lengths can be found in the original paper. In the present work, values of $h_{\min}$ and h_{des} equal to 5 and 30 m respectively were considered for the calculations. The leakage exponent n_{leak} in Eq. (8) was set to 1.18, as was done by Pezzinga and Pititto (2005). This value lies in the range [0.5, 1.5] of typical values and is mainly associated with the presence of longitudinal cracks in plastic pipes (Van Zyl and Cassa 2014). The choice of such a simple network as first case study is motivated by the necessity of facilitating the analysis of the results. This was done in light of the focus of the paper, which is to present expressions for assessing the resilience and failure indices in the pressure-driven modeling approach.

A first application was carried out to show how the resilience and failure indices proposed in this paper vary when leakage percentage changes. This was done by initially considering, for explicative purposes, a network configuration with uniform pipe diameters equal to 457.2 mm. To obtain different leakage outflows, pipe leak coefficients $C_{L,i}$ were modified uniformly in the network. In particular, the network leakage coefficient C_L was set to various values within the range $[5 \times 10^{-8}, 1 \times 10^{-6}]\mathrm{m}^{0.82}\ \mathrm{s}^{-1}$. Though the wide range adopted for C_L extends beyond the usual values of real water loss, it helps, on the one hand, in fully describing the unaccounted-for water, which also includes apparent losses such as theft, meter underregistration, unmetered users, flushing, firefighting. On the other hand, it enables clearly analyzing how the newly

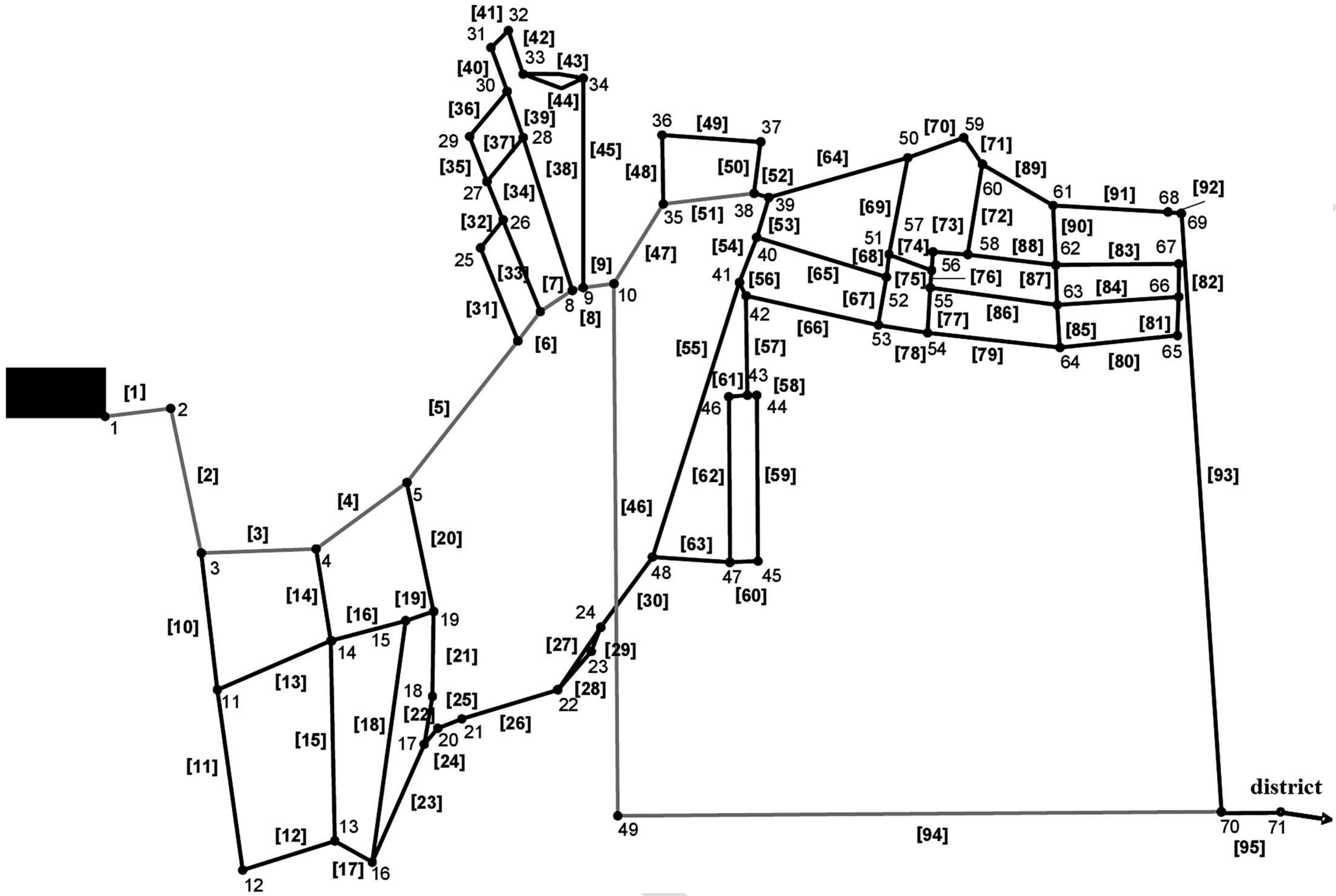

Fig. 3. Second case study: reference network of a town in northern Italy; node IDs close to the nodes; pipe IDs inside the brackets []; in Node 71, supply of a district

formulated resilience and failure indices react to nodal outflow variations.

As a second application, the two-objective design of the network was carried out to minimize the total network cost (sum of pipe costs) and maximize GRF. As in the original problem presented by Alperovits and Shamir (1977), the pipe sizes were considered the decisional variables for the design. In this work, the same pipe costs per unit length as a function of the pipe diameter, as those defined by Alperovits and Shamir (1977) without any cost unit, were used. In the context of the two-objective network design, an optimization was carried out using the NSGAII algorithm (Deb et al. 2002) and considering a uniform value $C_L = 5 \times 10^{-8}$ $\mathrm{m}^{0.82}$ s^{-1} in network pipes.

Fig. 4. Third case study: reference network of a city in northern Italy

The second case study of the paper concerned a network featuring $n_0 = 1$ source node, $n_1 = 70$ nodes with outflow and $n_p = 95$ pipes (Fig. 3). The network, which represents the water distribution system serving a town in northern Italy, features a total end-to-end length of about 14 km. The pipe and nodal characteristics of this network are reported in the work by Creaco et al. (2012). Unlike the latter work, in which the demands were allocated along the network pipes, in the present work they are allocated to the network nodes with unknown head. The whole network peak demand is 15 L/s, including about 20% of leakage. In the calculations, the pipe resistance was modeled through the Manning formula. Like in the first case study, the leakage exponent n_{leak} in Eq. (8) was set to 1.18. The network performance in terms of I_r and I_f (i.e., GRF) was analyzed in seven extended period scenarios, each of which aimed at representing the day of peak demand. The scenarios, aimed at representing various ages in the network, differed in the values of the network leakage coefficient C_L and of the pipe Manning roughness coefficient. As Table 1 shows, the scenarios, associated with growing network ages from 0 to 60 years, featured C_L values ranging

Table 1. Second Case Study: Network Age, Leakage Coefficient C_L, Leakage Percentage and Mean Pipe Manning Coefficient Associated with Each Scenario

Scenario	Age (years)	C_L ($m^{0.82}$ s^{-1})	Leakage percentage (%)	Mean manning coefficient ($m^{-1/3}$ s)
1	0	4.50×10^{-9}	29	0.0098
2	10	5.63×10^{-9}	33	0.0113
3	20	6.75×10^{-9}	37	0.0128
4	30	9.00×10^{-9}	44	0.0139
5	40	1.13×10^{-8}	49	0.0143
6	50	1.35×10^{-8}	53	0.0147
7	60	1.58×10^{-8}	57	0.0150

Table 2. Third Case Study: Network Age, Leakage Coefficient C_L, Leakage Percentage and Pipe Manning Coefficient Associated with Each Scenario

Scenario	Age (years)	C_L ($m^{0.82}$ s^{-1})	Leakage percentage (%)	Manning coefficient ($m^{-1/3}$ s)
1	0	1.56×10^{-8}	28	0.0100
2	10	1.95×10^{-8}	33	0.0115
3	20	2.34×10^{-8}	37	0.0130
4	30	3.12×10^{-8}	43	0.0145
5	40	3.90×10^{-8}	49	0.0150
6	50	4.68×10^{-8}	53	0.0150
7	60	5.46×10^{-8}	56	0.0150

from 4.5×10^{-9} $m^{0.82}$ s^{-1} (estimated value for the real network) to 1.58×10^{-8} $m^{0.82}$ s^{-1}. In each scenario, the Manning coefficient value of each pipe was obtained starting from the real one, reported by Creaco et al. (2012), by adding the quantity 0.00015× (network age)) up to a maximum value of 0.015 $m^{-1/3}$ s. This was done to account for pipe deterioration as time goes by. The trend of the hourly demand coefficient reported in Fig. 5 was assumed valid in all the scenarios.

The third case study of the paper concerned a network featuring $n_0 = 2$ source nodes, $n_1 = 536$ nodes with outflow and $n_p = 825$ pipes (Fig. 4). The network, which represents the water distribution system serving a part of a city in northern Italy (Creaco and Franchini 2012), features a total end-to-end length of about 90 km. In this network layout, all nodes have a ground elevation of 0 m a.s.l., and the two source nodes have heads at 30 m a.s.l. The whole network peak demand is 367 L/s, including about 20% of leakage. In the calculations, the pipe resistance was modeled through the Manning formula. Like in the other case studies, the leakage exponent n_{leak} in Eq. (8) was set to 1.18. Like in the second case study, the network performance in terms of I_r and I_f (i.e., GRF) was analyzed in seven extended period scenarios, representing the peak daily demand at various network ages. The differences between the scenarios in terms of leakage coefficient C_L and pipe roughness, both assumed uniform over the network, are shown in Table 2. The same trend of hourly demand coefficient (Fig. 5) as the second case study was also used for the third case study.

Results

First Case Study—Network Simulation

As far as the first case study is concerned, the leakage coefficient C_L variation within the range $[5 \times 10^{-8}, 1 \times 10^{-6}]$ $m^{0.82}$ s^{-1}

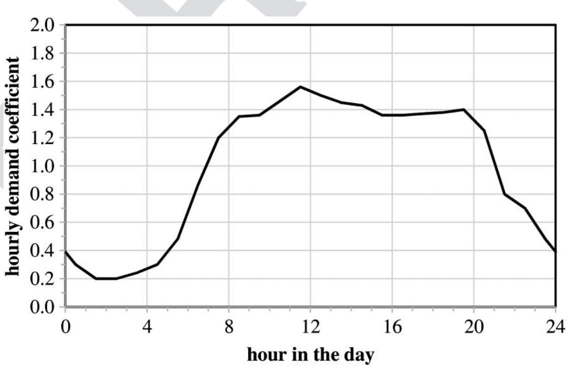

Fig. 5. Hourly demand coefficient used for the calculations in the second and third case studies

produced leakage percentage rates within the range [9–50%]. The results of the first part of the applications are reported in Fig. 6. Figs. 6(a and b) show how the resilience index I_r and the failure index I_f, as defined in this work, evaluated through the *pressure-driven modeling*, are affected by leakage increase. In particular, when the ratio of leakage to the whole outflow varies from about 9% to about 32% as a result of C_L variation, I_r decreases from 0.28 to 0.00. Starting from a leakage percentage equal to 32%, the network has no power surplus and starts to have power deficit. Therefore, for leakage percentages larger than 32%, I_r remains equal to 0. As for the failure index, I_f stays equal to 0 when leakage percentage varies from 9 to 32%. Then, it starts decreasing down to about −0.19 when leakage changes from 32 to 50%. Overall, Figs. 6(a and b) give a numerical proof of the continuity of I_r and I_f, which was shown in Fig. 1 in a qualitative way.

The behavior of I_r and I_f is because the nodal pressure heads and delivered powers decrease with the leakage outflow, and then the whole outflow $\mathbf{Q_0}$ [Eq. (14)] increasing. A comparison was then made between the resilience index I_r defined hereinbefore and that defined by Saldarriaga et al. (2010) [I_{rs} in Eq. (11)].

As Fig. 6(a) shows, I_{rs} takes on values within the range [0.7, 0.8]. These values are much larger than those of I_r, within the range [0, 0.3]. This happens because leakage appears in the numerator of I_{rs}. Therefore, the latter index provides an unrealistic estimate of the power supply delivered to the users. Furthermore, I_{rs} stays almost constant, not being strongly influenced by leakage increase. In particular, it increases a little bit up to a leakage percentage of about 25%. Then, after a plateau, it slightly decreases. The existence of these two trends depends on the fact that up to a leakage percentage of about 25%, the outflows to the users stay almost equal to the demands [see Fig. 6(c)] in Fig. 6 reporting performance indicator mean (q_{user}/d) related to the satisfaction of the users' demand). When leakage percentage further increases, the outflow to the users starts decreasing, because of some nodal pressure heads h being lower than h_{des}, and this results in a decrease in I_{rs}.

In the context of the comparison of I_r with I_{rs}, it is believed that, in light of its realistic estimate of the power supplied to the network users and due to its clearly decreasing trend as a function of leakage, I_r is closer to the original rationale used by Todini (2000) for defining the resilience index. In fact, the resilience index was conceived in order to yield indications of how much power reserve remains available in a certain network configuration, for facing eventual occurrence of critical scenarios still satisfying users' requests. Therefore, it is intuitive to think that an increase in leakage, and then in power dissipation through leakage, must always lead to a waste in the power reserve, and then to a decrease in the resilience index. This behavior is remarked in I_r and is missed by I_{rs}. In addition, the newly defined failure index I_f helps in providing

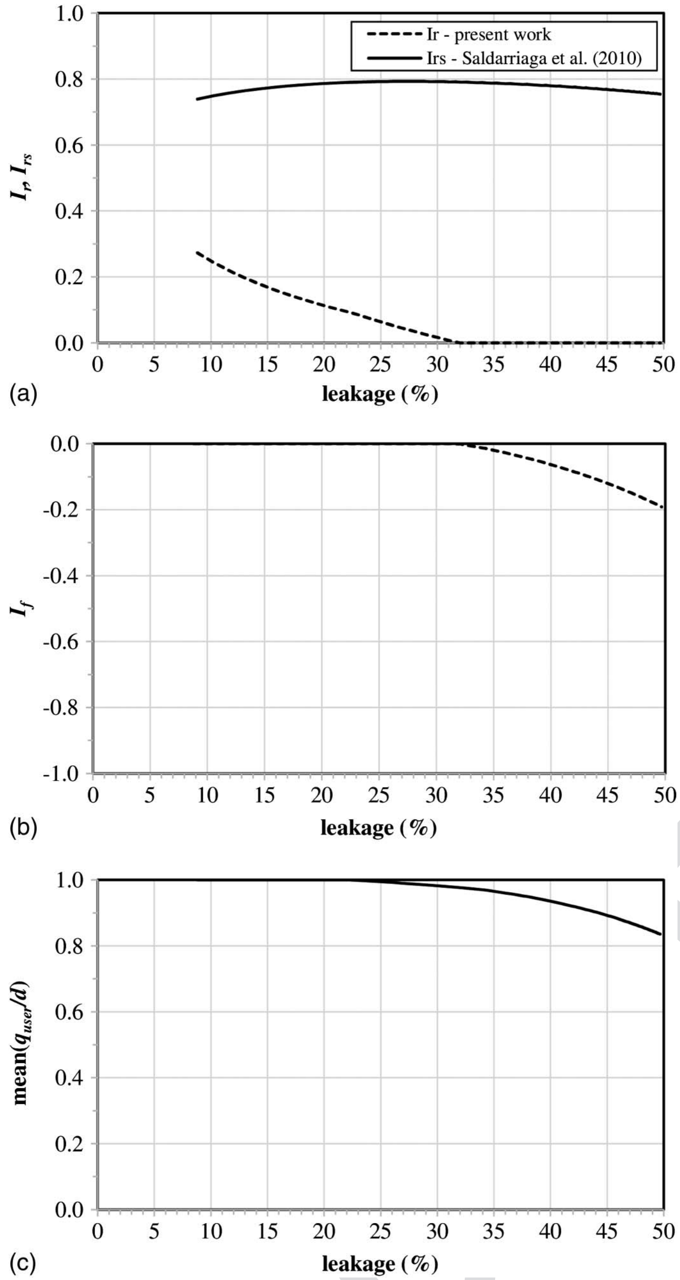

Fig. 6. First case study: as a function of leakage percentage compared to the whole outflow, trends of (a) resilience index, as was defined by Saldarriaga et al. (2010) (I_{rs}) and as is defined in this work (I_r); (b) failure index I_f as is defined in this work; (c) performance indicator mean (q_{user}/d)

information about the power content of network configurations under power deficit conditions.

First Case Study—Network Design

As for the second part of the applications, the results of the optimization is reported in the graphs in Fig. 7. Fig. 7(a) shows that, as expected, the Pareto front obtained in the optimization is limited between values of −1 and 1 of objective function GRF $= I_r + I_f$. Fig. 7(a) also shows the leakage percentage rate on the second vertical axis. This rate equals 100% in the optimization solution featuring GRF $= -1$, in which all nodal outflow is leakage and there is no flow delivered to users. As the network cost grows, it rapidly decreases up to a minimum value. Then, it grows rapidly

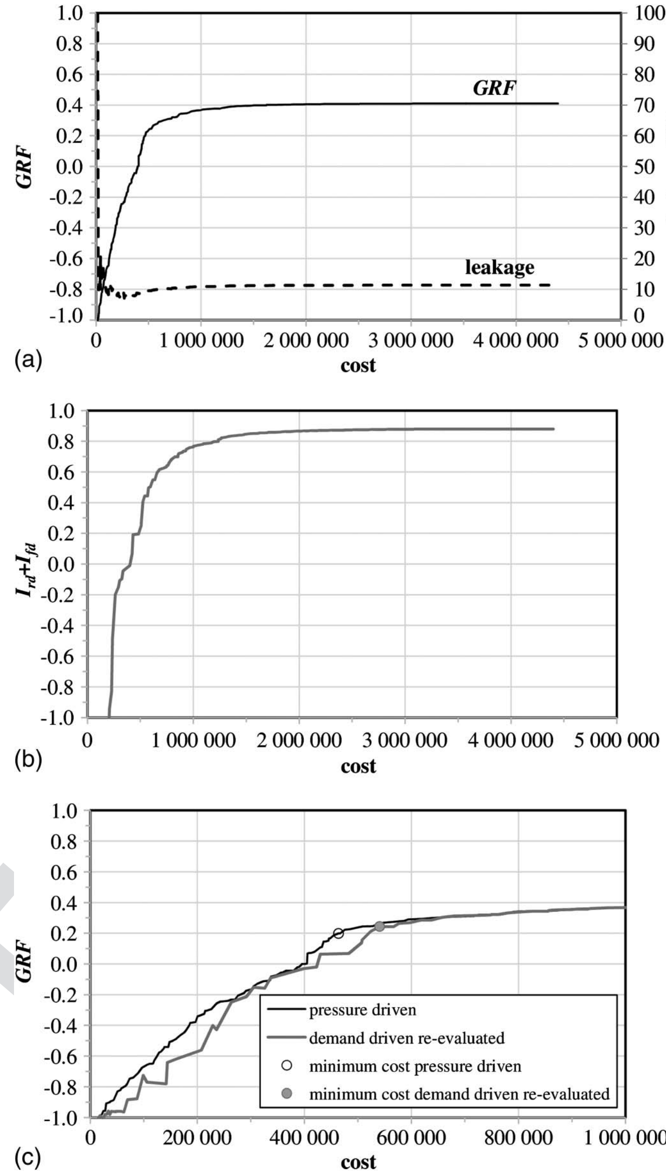

Fig. 7. First case study: (a) Pareto front obtained in the optimization and leakage percentage rate in the various solutions; (b) Pareto front obtained in the benchmark optimization (BO); (c) comparison between the optimization solutions and reevaluated BO solutions

again and stabilizes around a value close to 11%, which is also the average percentage rate over the optimization solutions. For the sake of comparison, a benchmark optimization (BO) where the resilience and failure indices were evaluated following the demand-driven approach [Todini 2000 Eqs. (9) and (10)] was carried out. In BO, nodal demands were then considered to be pressure independent. Compared to the users' demands in the optimization, the demands in BO were increased by 12%, in order to account, in all the BO solutions, for a constant (pressure independent) leakage rate of 11%, equal to the average leakage percentage over the optimization solutions. In fact, in the demand-driven approach (where $\mathbf{q} = \mathbf{d}$), leakage cannot be expressed as a function of nodal pressure heads and it has to be fixed *a priori* in an approximate way. The Pareto front obtained in BO was reported in Fig. 7(b). Unlike the Pareto fronts of the optimization, which only include values of GRF $= I_r + I_f$ larger than or equal to −1, the Pareto front of BO does not have a lower boundary (though the graph is bounded below by −1). This happens because nodal heads are not bounded below in demand-driven network simulations (nodal outflows do not decrease with service pressure decreasing). In pressure-driven simulations, instead, pressure heads cannot go below $h_{\min}$, as nodal outflows are set equal to 0 for $h < h_{\min}$. The highest value achieved by $I_{rd} + I_{fd}$ is close to 0.9, which is much larger than the highest value of GRF in Fig. 7(a). This difference happens because, by including leakage in the numerator, I_{rd} considers leakage outflows inside the good power delivered to the users. Therefore, $I_{rd} + I_{fd}$ is a wrong estimate of the real power delivered to the users. In order to be able to compare directly the optimization solutions (pressure-driven modeling) with the BO solutions (demand-driven modeling), the latter were reevaluated using the pressure-driven modeling. In particular, for each BO solution, a pressure-driven network simulation where nodal outflows were calculated considering Eqs. (4)–(8) was performed. The pressure driven–related I_r and I_f associated with each solution were then calculated through Eqs. (14) and (15), respectively. The reevaluated BO solutions were then plotted in terms of network cost and GRF $= I_r + I_f$ in Fig. 7(c), along with the optimization solutions. The comparison in this graph highlights the fact that the solutions of the benchmark optimization BO are dominated by the optimization solutions up to a network cost value close to 600,000. Furthermore, using the demand-driven approach and including leakage in an approximate way leads to wrong assessment of the minimum cost solution which guarantees $h > h_{\text{des}}$ at all nodes (cost = 541,000 from the benchmark optimization BO, instead of cost = 464,000 from the pressure-driven optimization). Fig. 7(c) shows that the GRF values of the optimization and BO solutions are closer (almost coincident) when the optimization solutions feature a leakage rate close to 11% [see Fig. 7(a)], which is equal to the constant pressure-independent leakage rate assumed in BO. More evident differences appear when the optimization solutions feature leakage percentage rates far from 11%. In general, for any value of leakage rate chosen for BO, the curve of reevaluated BO solutions is close to the optimization Pareto front in correspondence to the optimization solutions featuring a close leakage rate. Discrepancies occur in correspondence to the optimization solutions featuring a different leakage rate from that assumed in the BO optimization. In fact, it is not possible to pick a single value of leakage rate that enables the curve of reevaluated BO solutions to be close to the optimization Pareto front over the whole Pareto front length.

An analysis was then carried out to show that I_r would take on illogical values for power deficient network configurations, if the numerator in Eq. (14) were not bounded below by 0. In Fig. 8(a), the I_r value calculated through Eq. (13), which is unbounded below, was plotted against the network cost for the optimization solutions. This figure clearly shows that, without the lower boundary, I_r takes on illogical values smaller than −1 and larger than 1, for power deficient network configurations (i.e., network costs lower than 400,000). Unlike GRF [see Fig. 7(a)], the unbounded I_r is not a monotonic function of the network cost in the region of the power deficient network configurations. Fig. 8(b) shows the values of the unbounded I_f, obtained neglecting the min function in Eq. (15), for the optimization solutions. Unlike the unbounded I_r, the unbounded I_f has a regular monotonic trend. However, it features smaller (positive) variations (within the range [0, 0.11]) than GRF [see Fig. 7(a)] and this fact prevents it from properly differentiating the solutions with power surplus. The loss of physical meaning for the unbounded I_r and the small positive variations in the unbounded I_f corroborate the definition of I_r and I_f through Eqs. (14) and (15), respectively, in an attempt to represent network configurations with power surplus and deficit in a separate way. The remarks made previously also justify the introduction of the combined index GRF to express the network power surplus/deficit conditions.

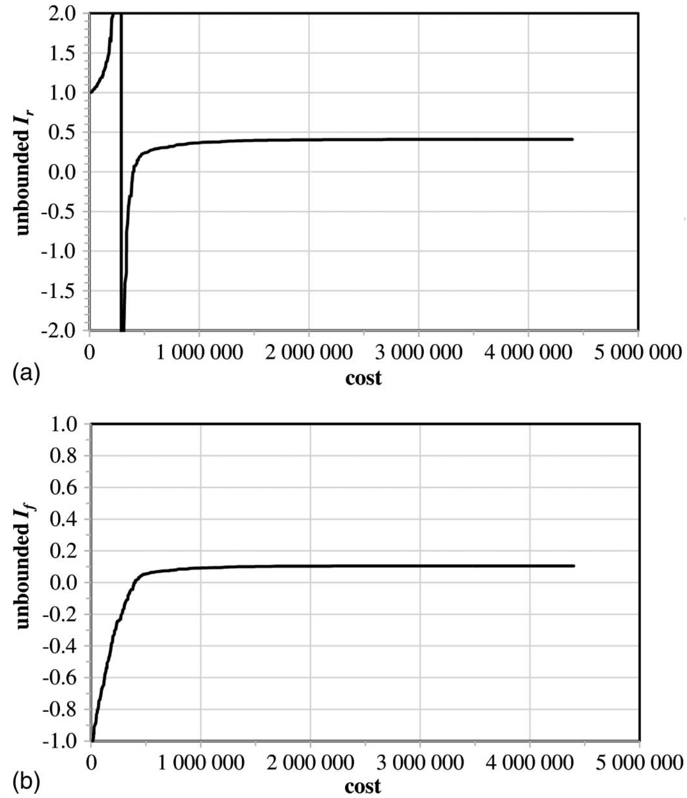

Fig. 8. (a) I_r and (b) I_f calculated neglecting the max and min function in Eqs. (14) and (15), as a function of network cost for optimization solutions

Second Case Study

As far as the second case study is concerned, the leakage percentage and the average value of the pipe Manning roughness coefficient obtained as a function of network age are reported in Table 1. The results of the analysis are plotted in the graphs in Fig. 9. In particular, Fig. 9(a) shows how GRF varies during the day in the various scenarios, which are representative of network aging and then feature growing values of pipe resistance (from the actual values up to 0.015 $\text{m}^{-1/3}$ s) and of leakage percentage (from the actual 29–57% of the total outflow). Overall, the daily trend of GRF tends to lower, as the network gets older. For network ages larger than 20 (i.e., in Scenarios 4–7), GRF even takes on negative values ($I_r = 0$ and $I_f < 0$), representative of power deficit. In all the scenarios, the values of GRF are always positive at nighttime since the network is always able to deliver sufficient power ($I_r > 0$ and $I_f = 0$) in this part of the day, which features low nodal demands. Furthermore, at nighttime GRF always takes on values close to 0 because of the low values of the power delivered to the users compared to the power leaving the source node (which also includes the power dissipated through leakage). Three different categories of scenario can be distinguished in Fig. 9(a). The first category includes Scenarios 1 and 2, in which GRF tends to be larger in the day than at nighttime. The second includes only Scenario 3, in which GRF is always close to 0 throughout the day. Finally, the third includes Scenarios 4–7, in which GRF tends to be lower in the day than at nighttime. The reason for the different behaviors of GRF lies in the fact that, in each scenario of the first category, the network power redundancy globally prevails over the network

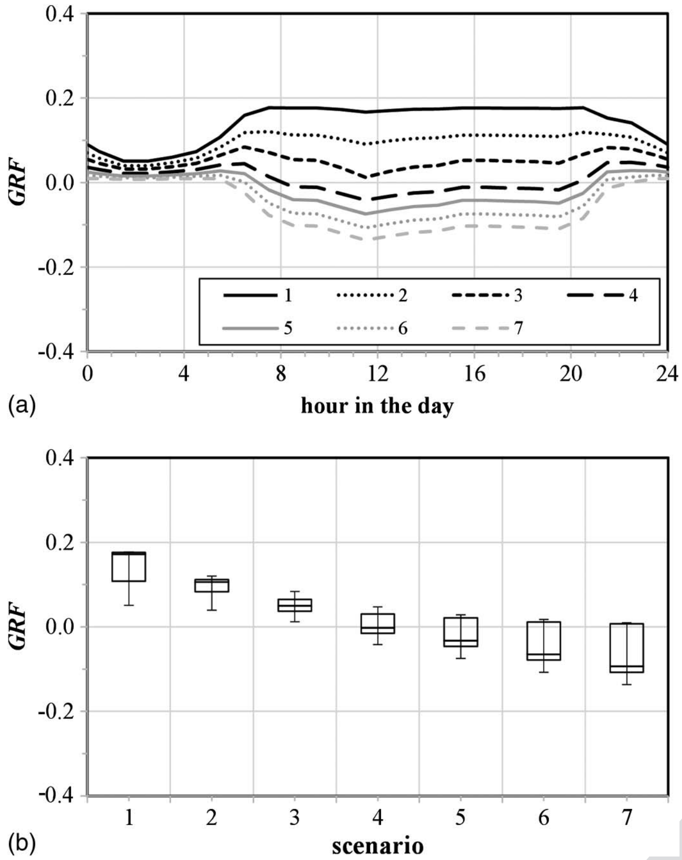

Fig. 9. Second case study: (a) index $\mathrm{GRF} = I_r + I_f$ during the day in the various scenarios; (b) for each scenario, box plot of the GRF values during the day

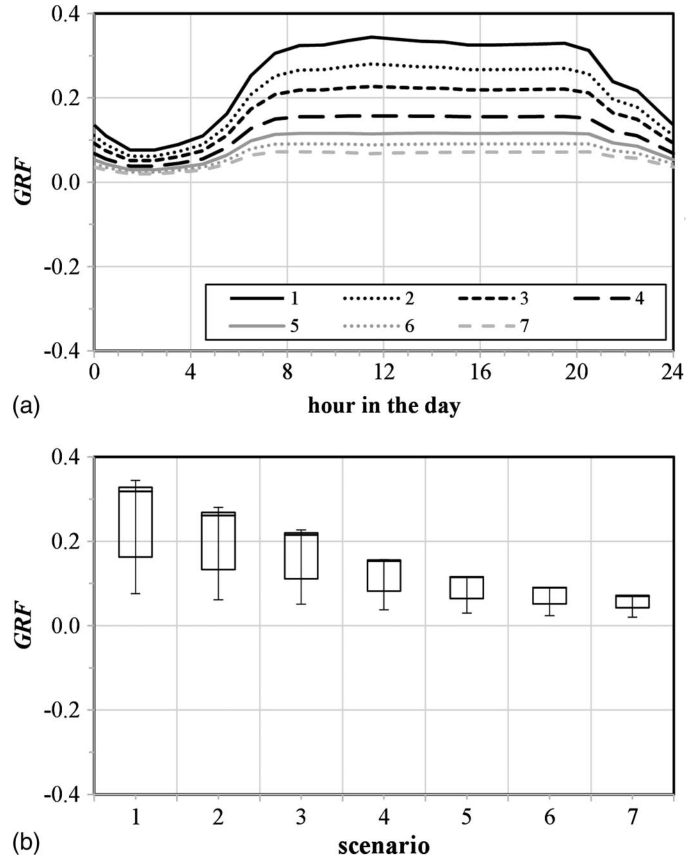

Fig. 10. Third case study: (a) index $\mathrm{GRF} = I_r + I_f$ during the day in the various scenarios; (b) for each scenario, box plot of the GRF values during the day

power deficit in terms of size and duration. In the scenario of the second category, the duration and size of network redundancy and deficit compensate for each other. Finally, in each scenario of the third category, the network deficit prevails over the network redundancy. Fig. 9(b) reports, for the each scenario, the box plot of the GRF values in the day. The analysis of the box plots shows that the GRF distribution tends to be very asymmetric with tail towards the lower values, symmetric and very asymmetric with tail towards the higher values, in the scenarios of the three categories defined previously, respectively. However, in the scenario of the second category, the variance is smaller than in the others. By summing up these results, all the scenarios feature most of the GRF values close to the median, which can then be considered as the most representative value of GRF to represent synthetically the power conditions in the network.

Third Case Study

As for the third case study, the leakage percentages obtained as a function of the network age are reported in Table 2. Figs. 10 (a and b) report, for the third case study, the same kind of results as Figs. 9(a and b), respectively. The main difference between the results of the two case studies lies in the fact that, in the third case study, GRF is always positive during the day in all the seven scenarios. Furthermore, according to the three categories of scenario defined previously, all the scenarios of the third case study belong to the first category, with distribution of GRF values very asymmetric with tail towards the lower values. The fact that the network in the third case study is never under power deficit conditions is due to the larger redundancy of the network in terms of loops and pipe sizes compared to the network of the second case study.

Conclusions

In this paper the resilience and failure indices, originally proposed by Todini (2000) using demand-driven modeling, were extended to pressure-driven modeling also accounting for leakage. This was done by defining a new generalized resilience/failure, following the original definition in terms of available and delivered power. Besides deriving pipe water discharges and nodal heads through pressure-driven modeling, the new formulation requires power loss due to leakage to be excluded from the power delivered to satisfy users demand. Applications to the WDN analysis showed that, thanks to the formulation adopted, the indices describe properly the variations in the power delivered to the users, as the ratio of leakage to whole network outflow changes. The generalized indices proved to be more sensitive to leakage variations than the pressure-driven resilience formulation proposed by Saldarriaga et al. (2010). Statistics on the index values can also be useful to analyze the network operation in an extended period simulation and the median appears to be the most representative value of GRF to describe synthetically the WDN power conditions. Applications to the multiobjective design in the presence of pressure-dependent outflow proved that considering the generalized indices yields benefits. In fact, network configurations are obtained, which dominate, in terms of cost and delivered power, those obtained using the indices evaluated through standard demand-driven modeling, where pressure dependent outflows are considered in an approximate way.

Summing up, in light of the current tendency to prefer the pressure-driven approach to the demand-driven one in the modeling of WDNs, it is expected that the generalized indices may replace the original ones in most applications.

References

Alperovits, E., and Shamir, U. (1977). "Design of optimal water distribution systems." *Water Resour. Res.*, 13(6), 885–900.

Alvisi, S., and Franchini, M. (2006). "Near-optimal rehabilitation scheduling of water distribution systems based on a multi-objective genetic algorithm." *Civ. Eng. Environ. Syst.*, 23(3), 143–160.

Atkinson, S., Farmani, R., Memon, F., and Butler, D. (2014). "Reliability indicators for water distribution system design: Comparison." *J. Water Resour. Plann. Manage.*, 10.1061/(ASCE)WR.1943-5452.0000304, 10.1061/(ASCE)WR.1943-5452.0000304, 160–168.

Ciaponi, C. (2009). "Performance analysis in water supply." *Performance indicators for the planning, design and management of water supply systems*, C. Ciaponi, ed., CSDU, Milano, 1–29.

Cimellaro, G., Tinebra, A., Renschler, C., and Fragiadakis, M. (2015). "New resilience index for urban water distribution networks." *J. Struct. Eng.*, 10.1061/(ASCE)ST.1943-541X.0001433, C4015014.

Creaco, E., and Franchini, M. (2012). "Fast network multi-objective design algorithm combined with an a posteriori procedure for reliability evaluation under various operational scenarios." *Urban Water J.*, 9 (6), 385–399.

Creaco, E., Franchini, M., and Alvisi, S. (2012). "Evaluating water demand shortfalls in segment analysis." *Water Resour. Manage.*, 26(8), 2301–2321.

Creaco, E., Franchini, M., and Todini, E. (2015). "The combined use of resilience and loop diameter uniformity as a good indirect measure of network reliability." *Urban Water J.*, 13(2), 167–181.

Creaco, E., Franchini, M., and Walski, T. (2014). "Accounting for phasing of construction within the design of water distribution networks." *J. Water Resour. Plann. Manage.*, 10.1061/(ASCE)WR.1943-5452.0000358, 598–606.

Creaco, E., and Pezzinga, G. (2015a). "Embedding linear programming in multi objective genetic algorithms for reducing the size of the search space with application to leakage minimization in water distribution networks." *Environ. Modell. Software*, 69, 308–318.

Creaco, E., and Pezzinga, G. (2015b). "Multi-objective optimization of pipe replacements and control valve installations for leakage attenuation in water distribution networks." *J. Water Resour. Plann. Manage.*, 10.1061/(ASCE)WR.1943-5452.0000458, 04014059-1-10.

Deb, K., Agrawal, S., Pratapm, A., and Meyarivan, T. (2002). "A fast and elitist multi-objective genetic algorithm: NSGA-II." *IEEE Trans. Evol. Comput.*, 6(2), 182–197.

Gargano, R., and Pianese, D. (2000). "Reliability as tool for hydraulic network planning." *J. Hydraul. Eng.*, 10.1061/(ASCE)0733-9429(2000)126:5(354), 354–364.

Germanopoulos, G. (1985). "A technical note on the inclusion of pressure dependent demand and leakage terms in water supply network models." *Civ. Eng. Syst.*, 2(3), 171–179.

Gessler, J., and Walski, T. M. (1985). "Water distribution system optimization." *Technical Rep. TREL-85-11*, U.S. Army Corps of Engineers' Waterways Experimentation Station, Vicksburg, MS.

Giustolisi, O., Kapelan, Z., and Savic, D. A. (2008a). "An algorithm for automatic detection of topological changes in water distribution networks." *J. Hydraul. Eng.*, 10.1061/(ASCE)0733-9429(2008)134:4(435), 435–446.

Giustolisi, O., Savic, D., and Kapelan, Z. (2008b). "Pressure-driven demand and leakage simulation for water distribution networks." *J. Hydraul. Eng.*, 10.1061/(ASCE)0733-9429(2008)134:5(626), 626–635.

Gupta, R., and Bhave, P. (1996). "Comparison of methods for predicting deficient-network performance." *J. Water Resour. Plann. Manage.*, 10.1061/(ASCE)0733-9496(1996)122:3(214), 214–217.

Mays, L. W. (1996). "Review of reliability analysis of water distribution systems." *Stochastic hydraulics '96*, Balkema, Rotterdam, 53–62.

Pandit, A., and Crittenden, J. C. (2012). "Index of network resilience (INR) for urban water distribution systems." *Proc., 2012 Critical Infrastructure Symp.*, Arlington, VA.

Pezzinga, G., and Pititto, G. (2005). "Combined optimization of pipes and control valves in water distribution networks." *J. Hydraul. Res.*, 43(6), 668–677.

Prasad, T. D., Sung-Hoon, H., and Namsik, P. (2003). "Reliability based design of water distribution networks using multiobjective genetic algorithms." *KSCE J. Civ. Eng.*, 7(3), 351–361.

Raad, D. N., Sinske, A. N., and van Vuuren, J. H. (2010). "Comparison of four reliability surrogate measures for water distribution systems design." *Water Resour. Res.*, 46(5), W05524.

Reddy, L. S., and Elango, K. (1989). "Analysis of water distribution networks with head dependent outlets." *Civ. Eng. Syst.*, 6(3), 102–110.

Saldarriaga, J. G., Ochoa, S., Moreno, M. E., Romero, N., and Cortés, O. J. (2010). "Prioritised rehabilitation of water distribution networks using dissipated power concept to reduce non-revenue water." *Urban Water J.*, 7(2), 121–140.

Tanyimboh, T. T., Tabesh, M., and Burrows, R. (2001). "Appraisal of source head methods for calculating reliability of water distribution network." *J. Water Resour. Plann. Manage.*, 10.1061/(ASCE)0733-9496(2001)127:4(206), 206–213 .

Todini, E. (2000). "Looped water distribution networks design using a resilience index based heuristic approach." *Urban Water*, 2(2), 115–122.

Todini, E., and Pilati, S. (1988). "A gradient algorithm for the analysis of pipe networks." *Computer applications in water supply*, B. Coulbeck, and C.-H. Orr, eds., ~~Wiley~~, 1–20.

Tucciarelli, T., Criminisi, A., and Termini, D. (1999). "Leak analysis in pipeline systems by means of optimal valve regulation." *J. Hydraul. Eng.*, 10.1061/(ASCE)0733-9429(1999)125:3(277), 277–285.

Van Zyl, J. E., and Cassa, A. M. (2014). "Modeling elastically deforming leaks in water distribution pipes." *J. Hydraul. Eng.*, 10.1061/(ASCE)HY.1943-7900.0000813, 182–189.

Wagner, J. M., Shamir, U., and Marks, D. H. (1988). "Water distribution reliability: Simulation methods." *J. Water Resour. Plann. Manage.*, 10.1061/(ASCE)0733-9496(1988)114:3(276), 276–294.

Walski, M., Chase, D., Savic, D., Grayman, W., Beckwith, S., and Koelle, E. (2003). *Advanced water distribution modelling and management*, Haestad, Waterbury, CT.

Queries

1. "The online citation name format is shown below. Please confirm each author's surname and first initial are shown correctly.- Creaco, E; Franchini, M; Todini, E"

2. Please provide the ASCE Membership Grades for the authors who are members.

3. [ASCE Open Access: Authors may choose to publish their papers through ASCE Open Access, making the paper freely available to all readers via the ASCE Library website. ASCE Open Access papers will be published under the Creative Commons-Attribution Only (CC-BY) License. The fee for this service is $1750, and must be paid prior to publication. If you indicate Yes, you will receive a follow-up message with payment instructions. If you indicate No, your paper will be published in the typical subscribed-access section of the Journal.]

4. Please check the hierarchy of section heading levels.

5. Please confirm that the large bracket is required at the left of Eq. (1).

6. Please check the caption to Fig. 1.

7. Please confirm citation of Fig. 7(a).

8. Please provide a unit for "costs lower than 600,000." Is this a U.S. dollar ($) value?

9. Please provide a unit for "541,000" and "464,000." Is these U.S. dollar ($) values?

10. please provide the unit for the value in the y-axis of Fig. 7. For example, are the values in U.S. dollars ($)?

11. Please provide a unit for "costs lower than 400,000." Is this a U.S. dollar ($) value?

12. please provide the unit for the value in the y-axis of Fig. 8. For example, are the values in U.S. dollars ($)?

13. Please provide complete publisher location for reference Ciaponi (2009).

14. A check of online databases year found in this reference. Please Add year '2014'.

15. Please provide the issue number for Ref. (Creaco and Pezzinga 2015b).

16. Please provide the publisher or sponsor name and location (not the conference location) for Ref. Pandit and Crittenden (2012).

17. This query was generated by an automatic reference checking system. This reference could not be located in the databases used by the system. While the reference may be correct, we ask that you check it so we can provide as many links to the referenced articles as possible.

18. Please provide the publisher's location for Ref. Todini and Pilati (1988).